MOLECULAR IMAGING AND BIOLOGY

Mol Imaging Biol (2019) 21:861–870
DOI: 10.1007/s11307-018-1235-6

Published Online: 21 February 2019

WMIS World Molecular Imaging Society

Check for updates

RESEARCH ARTICLE

Multimodality Hyperpolarized C-13 MRS/PET/Multiparametric MR Imaging for Detection and Image-Guided Biopsy of Prostate Cancer: First Experience in a Canine Prostate Cancer Model

Sunitha V. Bachawal,[1] Jae Mo Park,[1,2] Keerthi S. Valluru,[1] Mathias Dyrberg Loft,[1] Stephen A. Felt,[3] José G. Vilches-Moure,[3] Yamil F. Saenz,[3] Bruce Daniel,[1] Andrei Iagaru,[1] Geoffrey Sonn,[1,4] Zhen Cheng,[1] Daniel M. Spielman,[1] Jürgen K. Willmann[1,5]

[1]*Department of Radiology, Stanford University, Stanford, CA, USA*
[2]*Advanced Imaging Research Center, University of Texas Southwestern Medical Center, Dallas, TX, USA*
[3]*Department of Comparative Medicine, Stanford University, Stanford, CA, USA*
[4]*Department of Urology, Stanford University, Stanford, CA, USA*
[5]*Department of Radiology, Molecular Imaging Program at Stanford, School of Medicine, Stanford University, 300 Pasteur Drive, Room H1307, Stanford, CA, 94305-5621, USA*

Abstract

Purpose: To assess whether simultaneous hyperpolarized C-13 magnetic resonance spectroscopy (MRS)/positron emission tomography (PET)/multiparametric magnetic resonance (mpMR) imaging is feasible in an orthotopic canine prostate cancer (PCa) model using a clinical PET/MR system and whether the combined imaging datasets can be fused with transrectal ultrasound (TRUS) in real time for multimodal image fusion-guided targeted biopsy of PCa.

Procedures: Institutional Animal Care and Use Committee approval was obtained for this study. Canine prostate adenocarcinoma (Ace-1) cells were orthotopically injected into the prostate of four dogs. Once tumor engraftment was confirmed by TRUS, simultaneous hyperpolarized C-13 MRS of [1-^{13}C]pyruvate, PET (2-deoxy-2-[^{18}F]fluoro-D-glucose ([^{18}F]FDG), [^{68}Ga]NODAGA-SCH1), and mpMR (T2W, DWI) imaging was performed using a clinical PET/MR system. Multimodality imaging data sets were then fused with TRUS and image-guided targeted biopsy was performed. Imaging results were then correlated with histological findings.

Results: Successful tumor engraftment was histologically confirmed in three of the four dogs (dogs 2, 3, and 4) and simultaneous C-13 MRS/PET/mpMR was feasible in all three. In dog 2, C-13 MRS showed increased lactate signal in the tumor (lactate/totalC = 0.47) whereas mpMR did not show any signal changes. In dog 3, [^{18}F]FDG-PET (SUV_{mean} = 1.90) and C-13 MRS (lactate/totalC = 0.59) showed elevated metabolic activity in the tumor. In dog 4, [^{18}F]FDG (SUV_{mean} =

Electronic supplementary material The online version of this article (https://doi.org/10.1007/s11307-018-1235-6) contains supplementary material, which is available to authorized users.

Correspondence to: Jürgen Willmann; *e-mail:* willmann@stanford.edu

2.43), [^{68}Ga]NODAGA-SCH1 (SUV_{mean} = 0.75), and C-13 MRS (Lac/totalC = 0.53) showed elevated uptake in tumor compared to control tissue and multimodal image fusion-guided biopsy of the tumor was successfully performed.
Conclusion: Simultaneous C-13 MRS/PET/mpMR imaging and multimodal image fusion-guided biopsy is feasible in a canine PCa model.

Key words: Multimodality imaging, Transrectal ultrasound, Hyperpolarized MR spectroscopy, Multiparametric MRI, PET, Prostate cancer, Image fusion, Targeted biopsy

Introduction

Approximately 28,000 American men die of prostate cancer (PCa) each year [1]. Until recently, transrectal ultrasound (TRUS) had been the only widely available imaging technique for detecting PCa. Because ultrasound performs poorly in visualizing PCa, diagnosis is most commonly accomplished by ultrasound-guided prostate biopsy. Biopsy is not only painful but is often associated with increasing rates of infection [2] and can also lead to overdiagnosis of indolent cancers [3], and/or miss aggressive cancer cases [4].

Multiparametric magnetic resonance imaging (mpMRI) is revolutionizing PCa diagnosis [5]. Using a scoring system based on a combined evaluation of diffusion-weighted imaging (DWI), dynamic contrast-enhanced (DCE) MRI, and high-resolution T_2-weighted imaging [6, 7], mpMRI scoring strongly correlates with the presence of PCa. Fusion of MRI with ultrasound has now emerged as a powerful tool to enable image-targeted prostate biopsy [8, 9]. However, mpMRI misses ~20 % of all index lesions (which are the largest and most aggressive) in men undergoing prostatectomy [10], underestimating the size of cancer it detects [11], and up to 40 % of men with a normal MRI are found to have PCa on conventional biopsy [4].

Emerging metabolic and molecular imaging techniques such as hyperpolarized C-13 MR spectroscopic (MRS) imaging and positron emission tomography (PET) using PCa-targeted PET tracers enable *in vivo* imaging of key metabolic and molecular features of PCa and may further improve accuracy of PCa imaging. Hyperpolarized C-13 MRS imaging is a technology which achieves a dramatically enhanced signal-to-noise ratio (SNR > 50,000-fold increase) [12] over conventional MRS imaging using a technique called dynamic nuclear polarization (DNP) in combination with a rapid dissolution process [13]. C-13 MRS enables *in vivo* imaging of key metabolic pathways *via* intravenous administration of a hyperpolarized C-13 agent [14]. [1-^{13}C]Pyruvate ([1-^{13}C]Pyr) and its downstream products lactate (Lac) and bicarbonate (Bic) occupies a key branch point in energy metabolism and is the most studied hyperpolarized substrate to date with one of the most prominent applications being cancer [15, 16]. Preclinical studies following administration of hyperpolarized [1-^{13}C]Pyr have shown that the [1-^{13}C]Lac labeling (indicated by [1-^{13}C]Lac/[1-^{13}C]Pyr ratio) increases with PCa grade and disease progression and decreases after anti-cancer therapy in a transgenic prostate adenocarcinoma mouse model [17]. Results from the first-in-human clinical trial using hyperpolarized Pyr in patients with PCa showed that the technique was safe, with no dose-limiting toxicities observed, and allowed distinguishing tumor, normal prostate, and blood vessels by elevated [1-^{13}C]Lac/[1-^{13}C]Pyr ratios in biopsy-proven tumor regions [16].

Similarly, recent PET imaging studies with PCa biomarkers including prostate-specific membrane antigen (PSMA) and gastrin-releasing peptide receptor (GRPR), both of which are significantly overexpressed in PCa compared to benign prostate hyperplasia (BPH) or prostatitis, suggest that they are promising targets for primary and metastatic PCa detection [18].

Despite major technological advances in those emerging imaging techniques, no single imaging modality currently performs well enough to eliminate the clinical problem of overdiagnosis of indolent PCa and underdiagnosis of aggressive PCa. We hypothesize that combination of complementary imaging modalities may improve our ability to image and characterize PCa. With a clinical polarizer recently installed adjacent to a clinical PET/MR scanner, hyperpolarized C-13 MRS, PET, and mpMRI performed in a single exam became possible in our department. To the best of our knowledge, no study has yet addressed whether multimodality hyperpolarized C-13 MRS/PET/mpMRI using a clinical PET/MR scanner is feasible in a large animal PCa model, which would be required for eventual clinical translation and testing of this imaging approach in patients.

The purpose of this study was to assess whether simultaneous hyperpolarized C-13 MRS/PET/mpMR imaging is feasible in an orthotopic canine PCa model using a clinical PET/MR system and whether the combined imaging datasets can be fused with TRUS in real time for multimodal image fusion-guided targeted biopsy of PCa.

Materials and Methods

Canine PCa Model

The Institutional Animal Care and Use Committee approved all procedures in this study. In all animals, an

orthotopic canine PCa model was established as described [19] with modifications. In brief, animals were immunosuppressed by oral administration of cyclosporine (20 mg/kg). Serum cyclosporine levels were monitored biweekly to achieve therapeutic levels of at least 400 ng/dl maintained throughout the study. Once therapeutic cyclosporine levels were established, a midline infra-umbilical laparotomy was performed and the prostate was exposed for tumor cell injections. To control needle placements within the prostate during cell injections, a clinical C10-4ec (4–10 MHz; Philips) curved array transducer connected to a clinical ultrasound scanner (EPIQ7; Philips) was placed transrectally. Under ultrasound guidance, Ace-1 cells (20×10^6 cells in first dog; 60×10^6 cells in remaining three dogs) [19], suspended in 0.2 ml of basement membrane matrix (Matrigel; BD Biosciences), were then randomly injected in one of the two prostate lobes using a 21-22G needle, leaving the non-injected lobe as intra-animal control tissue. The needle was kept in place for 30 s and a cotton swab was immediately applied to minimize cell leakage while removing the needle. Saline irrigation was performed prior to three-layer abdominal wall closure. Tumor cell injections were successful in all animals, and all animals recovered well without any side effects. Successful tumor engraftment was observed in all animals with the implantation of 60×10^6 cells. When only 20×10^6 cells were injected, no distinct tumor growth was observed; therefore, this animal (dog 1) was excluded from subsequent analysis. Further details on the surgical preparation and post-surgical care are provided in Supplementary Materials.

Study Protocol

The first PET/MR imaging feasibility study using simultaneous hyperpolarized [1-^{13}C]Pyr and 2-deoxy-2-[^{18}F]fluoro-D-glucose ([^{18}F]FDG) PET was done by Gutte H et al., in dogs with spontaneous malignant tumor [15, 20]. This preclinical proof-of-principle study was designed to show the feasibility of simultaneous hyperpolarized C-13 MRS/PET/mpMR imaging and image fusion-guided transrectal biopsy of the prostate using clinical imaging equipment in a large animal model of PCa. The overall study design is summarized in Fig. 1 and involved TRUS-guided implantation of orthotopic PCa followed by monitoring the tumor growth using TRUS approximately 1 week after surgery. Once the tumor growth was confirmed, simultaneous hyperpolarized C-13 MRS/PET/mpMR imaging was performed (~2 weeks after surgery), followed by multimodality-image fusion with TRUS to test the feasibility of performing a targeted biopsy. Targeted biopsy was performed 48 h after simultaneous hyperpolarized C-13 MRS/PET/mpMR imaging to allow the PET tracer to decay.

Simultaneous Hyperpolarized C-13 MRS/PET/mpMR Imaging and Data Analysis

All PET/MR imaging was performed on a clinical 3T PET/MR scanner (SIGNA™; GE-Healthcare) approximately 2 weeks after tumor inoculation. Refer to Supplementary Materials for further details.

PET Imaging Synthesis of the radiotracers and the ligand-binding assay are descried under Supplementary methods. Dynamic 2-deoxy-2-[^{18}F]fluoro -D-glucose ([^{18}F]FDG) (74 MBq; diluted in 2.5 ml saline, half-life = 110 min) time-of-flight (TOF) PET scanning of the lower pelvic area with endorectal and clamshell coils in place was performed in three dogs. In one animal, 4 h prior to [^{18}F]FDG-PET imaging, dynamic [^{68}Ga]NODAGA-SCH1 (74 MBq; diluted in 2.5 ml saline, half-life = 68 min) was performed as well. All PET acquisitions were performed in three-dimensional mode to obtain 89 slices per animal and lasted 2 h. The dynamic PET data for both [^{18}F]FDG and [^{68}Ga]NODAGA-SCH1 scans were reconstructed in 10-min bins using an iterative ordered subset expectation maximization (OSEM) algorithm (24 subsets, 3 iterations as recommended by the manufacturer). The coil attenuation was not taken into account for the PET reconstruction. Using ImageQC software available on the GE PET/MR console, circular regions of interest (ROI) corresponding to prostate cancer (diameter, 0.5–1.5 cm) were marked on transverse PET/MR images with an ROI of a similar size marked on the contralateral control normal side of the prostate. Thereafter, the lesion and contralateral control prostate tissue ROIs were evaluated to determine the mean and maximum standardized uptake values (SUVs).

Multiparametric MR Imaging Concurrent to the PET scan, a volumetric T1-weighted acquisition with fat-water separation and motion correction to enable free-breathing (MRAC; TE1/TE2//TR = 1.674/2.232/4.045 ms; flip angle = 5°; FOV = 375 × 375 mm^2; 120 slices; slice thickness = 5.2 mm) was first obtained using the H-1 body coil and used for the generation of attenuation maps and for anatomic allocation of the PET results. mpMRI acquisition was then performed which involved the collection of 3D T2W (FSE, TE/TR = 157.5/2000 ms, flip angle = 90°; echo train length = 96; FOV = 160 × 160 × 120 mm^3; matrix size = 288 × 224 × 120), and FOV optimized and constrained undistorted single shot (FOCUS) small FOV diffusion-weighted imaging (DWI, TE/TR = 68.7/2000 ms; FOV = 45 × 11.25 mm^2; matrix size = 160 × 80; slice thickness = 4.2 mm; 13 slices; 16 averages; *b*-value = 0, 25, 50, 800, and 1200 s/mm^2) pulse sequences. All T2W images were evaluated qualitatively in terms of signal intensity in tumors compared to contralateral prostate tissue.

C-13 Hyperpolarized MRS Imaging Hyperpolarized C-13 MRS imaging was performed while the dynamic PET scan was still running. 0.8 ml/kg body weight of 250-mM hyperpolarized [1-^{13}C]Pyr was injected intravenously, followed by C-13 MRS acquisition over 19 s using a single-slice, single-time point free-induction decay chemical shift imaging (FID-CSI, flip angle = 10°, FOV = 80 × 80 mm^2; matrix size = 16 × 16) sequence, starting 25 s after bolus injection [16]. Hyperpolarized C-13 MRS data were reconstructed using MATLAB (Mathworks, Natick, MA). The raw data were apodized by a 30-Hz Gaussian filter and zero-filled by a factor of 4 in spectral domain. Then, the processed data were further apodized by a generalized Hamming window with $\alpha = 0.66$, and zero-filled by a factor of 4 in the spatial domains, followed by 3D fast Fourier transform. Metabolite maps were quantified by integrating the respective peak in absorption mode after zero-order phase correction [17]. To compensate the inhomogeneous detection profile of C-13 endorectal coil, [1-^{13}C]Pyr and [1-^{13}C]Lac maps were normalized by the sum of all the C-13-labeled metabolite maps, which are [1-^{13}C]Pyr, [1-^{13}C]Pyr-hydrate, [1-^{13}C]alanine, [1-^{13}C]Bic, and [1-^{13}C]Lac (referred to as totalC).

Multimodal Image Fusion with Real-time Transrectal Ultrasound and Targeted Biopsy of PCa

Multimodal fusion of hyperpolarized C-13 MRS/PET/mpMR images with TRUS (EPIQ 7, C10-4ec transrectal curved array transducer; Philips) was performed using commercially available software (PercuNav, Philips) (Supplementary Materials). The feasibility of image fusion-guided targeted biopsy was tested in one animal. For this purpose, a standard spring-loaded gun (BARD MAGNUM, Murray Hill, NJ) with 18G × 25 cm needle (sample notch, 1.9 cm) was used and inserted transrectally using a needle guide on the ultrasound transducer. After determining tumor location, a guided biopsy was performed and sample was processed for histopathological evaluation. *Ex vivo* histological analysis of the prostate samples was performed using standard procedures (Supplementary Materials).

Statistical Analysis

Continuous measurements for *in vitro* experiments were reported as mean ± standard deviation. Four dogs were considered sufficient for this study to achieve an appropriate tradeoff between cost and minimal sufficient number of animals to pilot the imaging, data processing, and image-fusion protocols to ensure reliable procedures for planned future human studies.

Results

Simultaneous Hyperpolarized C-13 MRS/PET/mpMR Imaging in Phantom

Ge-68 phantom experiments showed that the clamshell coil resulted in a PET signal degradation of approximately 15 % (Fig. 2). CT-based attenuation correction was therefore incorporated into the PET reconstruction, resulting in improved image contrast both in phantom and *in vivo* (Fig. 2). Attenuation-corrected simultaneous C-13 MRS/PET/mpMR imaging was feasible in all animals. In hyperpolarized MRS imaging, [1-^{13}C]Pyr, [1-^{13}C]Pyr-hydrate, and [1-^{13}C]Lac were detected from all the subjects. [1-^{13}C]Alanine and [1-^{13}C]Bic peaks were, however, below noise level.

In Vitro Validation of GRPR Expression in Ace-1 Cells

In order to perform Ga-68-based GRPR-targeted PET imaging, Ace-1 cells were tested for GRPR expression using receptor-binding assay with a radioligand, [^{125}I][Tyr4] BBN. Results confirmed that Ace-1 cells have very high GRPR expression with up to $1.58 \pm 0.24 \times 10^8$ GRPR receptors per cell.

In Vivo Multimodal Imaging

To test the feasibility of detecting prostate cancer using multimodal imaging, hyperpolarized C-13 MRS, PET, and mpMR imaging were performed simultaneously in an orthotropic canine model. Table 1 provides the summary of imaging performed in each animal.

mpMRI: In all animals, the prostate appeared overall heterogeneous on T2W MR images with no restricted diffusion on DW images. In dog 4, there was a distinct hypointense lesion with a hyperintense center corresponding to a tumor nodule as seen on histology.

Hyperpolarized C-13 MRS Overall, in all animals, an elevated metabolic activity with increased lactate conversion was observed in the tumor area compared to surrounding/contralateral normal prostate tissue. In addition, there were small areas of increased lactate signal on the left anterior circumference in the contralateral prostate lobe in dog 3 (Fig. 3) and dog 4 (Fig. 4) that corresponded to moderate to severe neutrophilic inflammation on the histology. The lactate conversion ratio for each corresponding histological feature in all animals is listed in Table 2.

PET Imaging [^{18}F]FDG uptake was increased in tumors of both the animals (dog 3 and dog 4) with SUV_{mean} and SUV_{max} of 1.90 and 2.21 in dog 3; and 2.43 and 2.82 in dog 4 compared to their respective contralateral control prostate

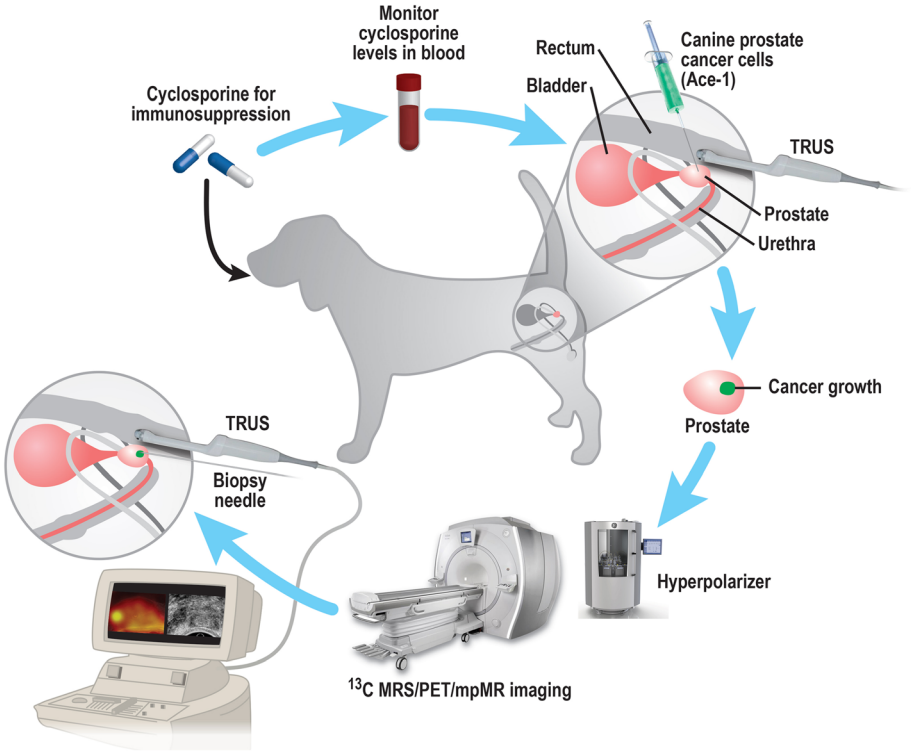

Fig. 1. Overall study design. Following immunosuppression, canine prostate adenocarcinoma Ace-1 cells were orthotopically injected under TRUS guidance into one of the prostate lobes. Following confirmation of tumor growth by TRUS, simultaneous hyperpolarized C-13 MRS/PET/mpMR imaging was performed. Multimodal data were fused with TRUS in real time and guided biopsy was performed.

tissue where the SUV_{mean} and SUV_{max}, were 1.23 and 1.67 for dog 3; SUV_{mean} and SUV_{max} for dog 4 was 1.40 and 1.35, respectively. Similarly, an increase in [^{68}Ga]NODAGA-SCH1 uptake was observed in tumors with SUV_{mean} of 0.75 and SUV_{max} of 0.86 in the tumor (*vs.* 0.38 and 0.58, respectively, in the contralateral control lobe).

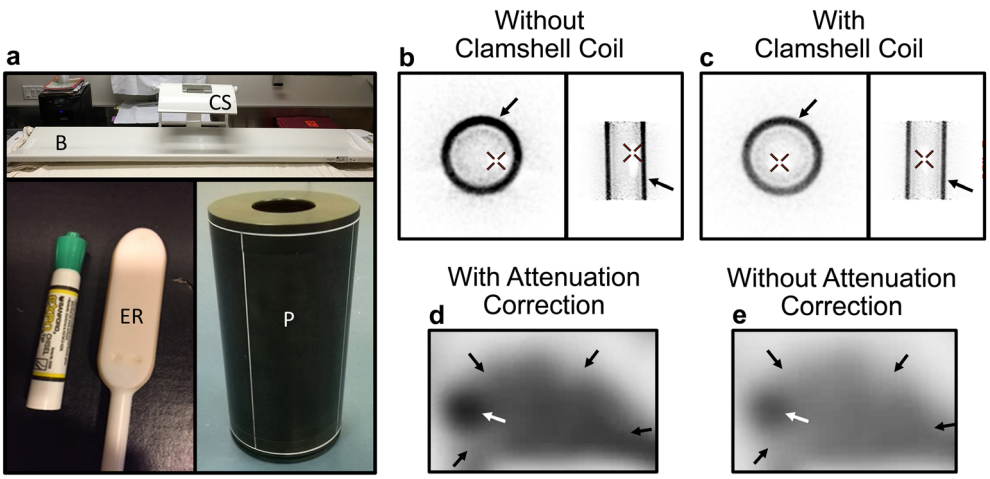

Fig. 2. Effect of clamshell C-13 transmit coil on PET image quality. **a** Photographs showing clamshell volumetric C-13 transmit coil (CS), patient bed (B), endorectal H-1/C-13 receiver coil (ER; active receiver area = 10 cm × 2.5 cm, length of the coil = 30 cm), and Ge-68 PET annulus phantom (P; diameter = 15 cm, length = 30 cm) used for coil calibration. PET images of the Ge-68 phantom (arrows; shown in transverse and longitudinal views each) **b** without the endorectal coil (position marked by X) inserted into the phantom and **c** with the coil inserted which illustrates decreased PET signal when the clamshell coil was used. The attenuation profile of the clamshell coil was subsequently determined with a CT scan (not shown) and was imported onto the PET/MR scanner for subsequent attenuation-corrected *in vivo* studies. Transverse PET images of a canine prostate (black arrows) with focal [^{18}F]FDG uptake in tumor (white arrow) in right prostate lobe show improved image contrast **d** with attenuation correction compared to **e** without attenuation correction.

Table 1. Summary of imaging performed in each animal

Animal no.	Tumor cell	Tumor growth	mpMRI	C-13 MRS	PET		Image fusion	Targeted biopsy
					[^{18}F]FDG	[^{68}Ga]NODAGA-SCH1		
Dog 1	20×10^6	No tumor	–	–	–	–	–	–
Dog 2	60×10^6	Scattered tumor clusters	+	+	–	–	+	–
Dog 3	60×10^6	Distinct tumor	+	+	+	–	+	–
Dog 4	60×10^6	Distinct tumor	+	+	+	+	+	+

Histological Findings

Histological evaluation of the tumor showed that tumor cells formed small-scattered nests and clusters of tumor cells along with severe inflammation in dog 2. In dog 3 and dog 4, a distinct tumor with a central necrotic core was confirmed. Also, in the contralateral prostate lobe in dog 3 and 4, moderate to severe neutrophilic inflammation was noted on histology, suggesting acute prostatitis (Figs. 3 and 4).

Multimodal Image Fusion with Real-time B-Mode Ultrasound Imaging and Fusion-Guided Targeted Biopsy

Multimodal image fusion was feasible in all dogs. The fusion procedure including importing the PET/MR images onto the ultrasound system and image alignment lasted for a maximum 5 min. Following image fusion, a successful image fusion-guided targeted biopsy of the prostate tumor was performed in dog 4 (Fig. 5) with histology confirming PCa.

Discussion

In this study, we showed that simultaneous hyperpolarized C-13 MRS/PET/mpMR imaging is feasible using a clinical PET/MR system along with successful multimodal image fusion-guided TRUS biopsy in a canine model of PCa. The imaging protocol optimized in this multimodal imaging study will lay a foundation for clinical translation to patients.

Imaging and needle biopsy play a critical role in diagnosis, prognostication, and treatment planning for PCa. An unmet clinical need exists to improve non-invasive techniques that improve detection of aggressive cancer and reduce overdiagnosis of indolent cancers. Simultaneously performed multimodal imaging can potentially fill this gap by complementing the strengths of each modality employed, and, when integrated with TRUS, improve performance of targeted cancer biopsy.

As a first step towards clinical translation of this multimodal imaging strategy, we tested feasibility of this approach in a large animal model of PCa. Dogs are well-established models for PCa research due to anatomical and

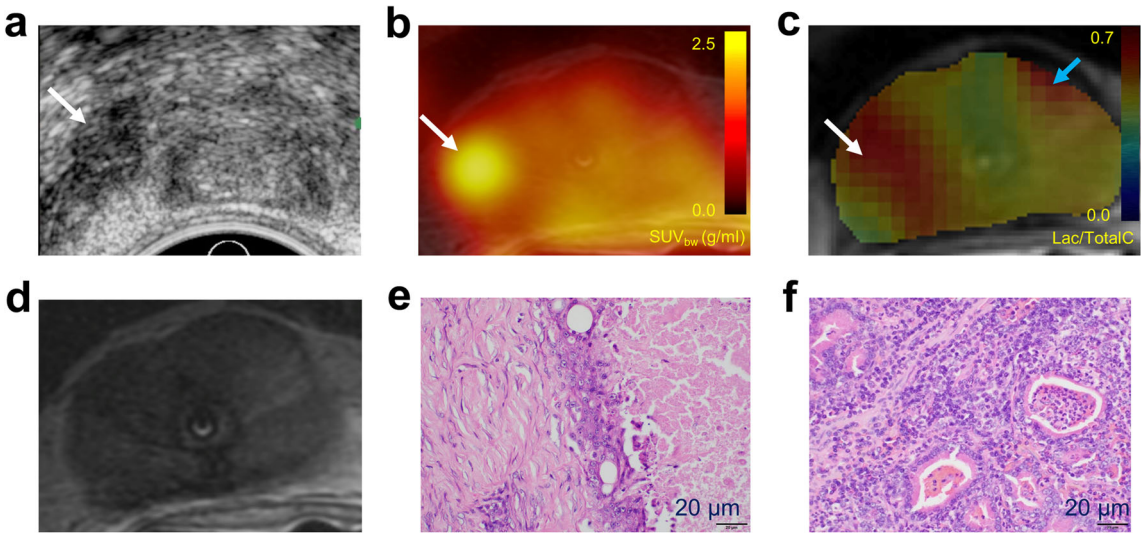

Fig. 3. Representative multimodality images of the prostate of dog 3. **a** Tumor growth was confirmed on transrectal ultrasound as hypoechoic lesion in the right prostate lobe (arrow) with **b** focal uptake of [^{18}F]FDG on reconstructed transverse PET image summed over 10 min starting at 50 min (arrow), and **c** increased conversion of pyruvate to lactate (white arrow) on transverse hyperpolarized MR spectroscopic image (overlaid on T2 image), 15 days after ultrasound imaging. **d** No discrete lesion was seen on transverse T2 image. **e** Histology showed tumor engraftment in the corresponding right prostate lobe. Note that there was also increased lactate signal in the contralateral prostate lobe (**c**, blue arrow) with **f** histology showing severe inflammation, suggesting acute prostatitis.

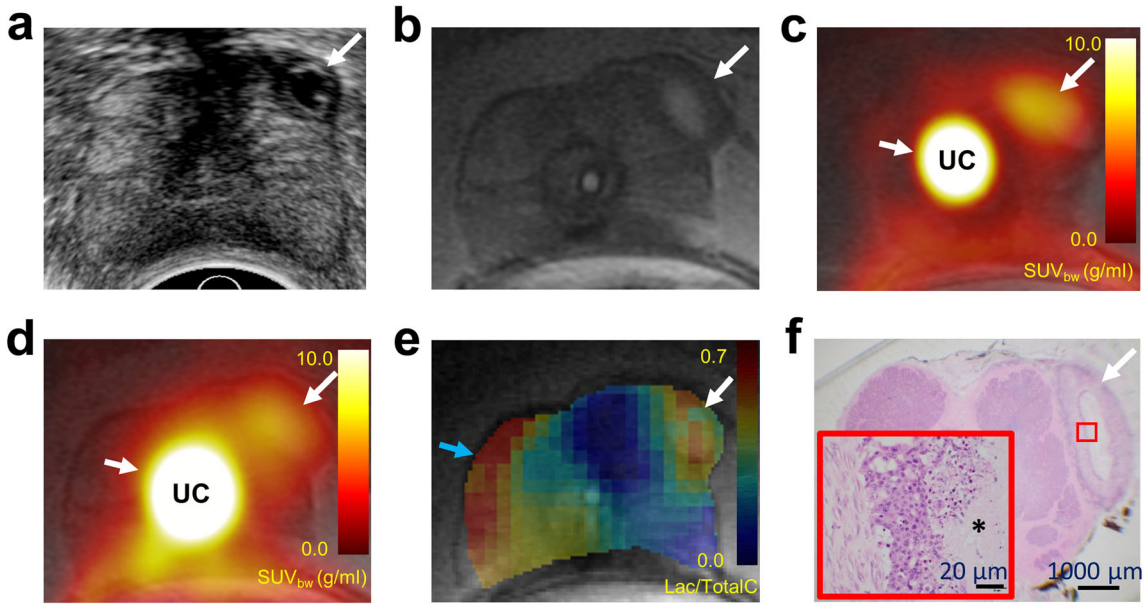

Fig. 4. Representative multimodality images of the prostate of dog 4. **a** On transrectal ultrasound, tumor engraftment was confirmed as hypoechoic lesion (arrow) with a central anechoic cystic component at the left anterior circumference of the prostate. Fourteen days after ultrasound imaging, multimodality imaging was performed: **b** on transverse T2 image, tumor showed a hypointense peripheral rim and a hyperintense center. Tumor also demonstrated both **c** [^{18}F]FDG and **d** [^{68}Ga]NODAGA-SCH1 uptake on reconstructed transverse PET images summed over 10 min starting at 50 min for [^{18}F]FDG, and 70 min for [^{68}Ga]NODAGA-SCH1 (arrows) as well as **e** increased lactate signal on transverse hyperpolarized MR spectroscopic image (white arrow). Increased lactate signal was also seen at the anterolateral circumference of the contralateral control prostate lobe (blue arrow). **f** Macroscopic whole prostate image (scale = 1 mm) and photomicrograph (inset in **f**; scale = 20 µm) confirmed tumor with central necrosis (black asterisk in inset). Note, strong PET signal artifact from urine due to blocked urinary catheter (UC) in urethra.

functional similarities of canine and human prostates including the size and location of a circumferential bilobed single gland [21]. Male dogs are the only non-primate large mammals besides humans to spontaneously develop BPH and PCa [22, 23]. While spontaneous canine cancer may reflect the biology of PCa development in human patients, it is difficult to obtain those dogs and PCa in them is typically detected at an advanced stage. Therefore, we used a recently described canine PCa model derived by orthotopically injecting canine prostate adenocarcinoma cells in immunosuppressed male beagles [19]. This allowed generating a well-controlled PCa model within 1 week after injecting 60 million tumor cells (with no tumor growth when only 20 million cells were injected), thereby decreasing cost and allowing better planning of experiments. To make the model more reliable in our hands, we incorporated some notable changes in our immunosuppression technique compared to the previously described approach [19]. Specifically, instead of administering a single cyclosporine dose per day varying between 12 and 40 mg/kg, we reduced the oral administration dose to 10 mg/kg and increased the administration frequency to twice a day and noticed that the cyclosporine target levels reached 600 to 1000 ng/dl within 10 days and remained stable throughout the experiments with few to no side effects observed in all dogs. We also preferred TRUS-guided direct manual injection after laparotomy over

Table 2. Normalized hyperpolarized C-13 MRS data with corresponding histology

Animal no.	Normalized hyperpolarized C-13 MRS data		Corresponding histology
	Lac/total C	Pyr/total C	
Dog 2	0.47	0.5	Tumor
	0.36	0.59	Surrounding normal
Dog 3	0.59	0.39	Tumor
	0.4	0.55	Surrounding normal
	0.62	0.35	Moderate to severe inflammation suggesting acute prostatitis
Dog 4	0.53	0.43	Tumor
	0.38	0.58	Surrounding normal
	0.6	0.37	Severe inflammation with acute prostatitis

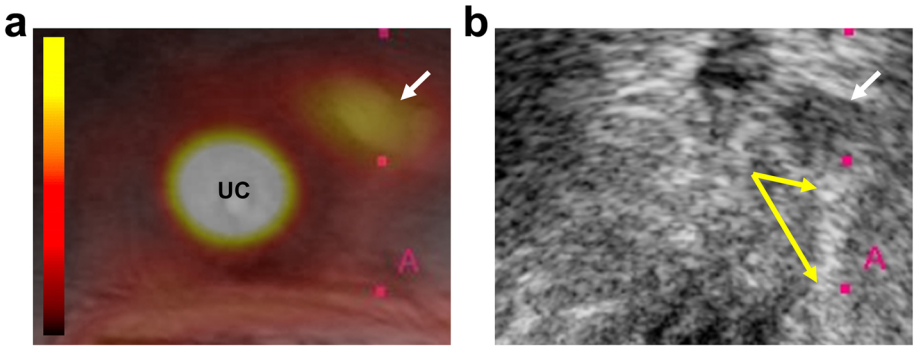

Fig. 5. Image fusion and guided biopsy of prostate tumor in dog 4. **a** PET/MR image was fused with ultrasound in real time and **b** image-guided biopsy was performed. Note needle guide (red dots) and biopsy needle (arrows) passing through the tumor. UC = urinary catheter with strong PET signal artifact from urine due to blocked catheter in urethra.

transabdominal percutaneous needle injections to gain more control over the tumor implantation procedure as the prostate in dogs is mobile as opposed to humans [24], necessitating manual fixation of the gland during needle insertion. Another notable change was to suspend the tumor cells in a basement membrane matrix with the goal of creating a plug after injection, reducing the possibility of cellular efflux into the urethra, and augmenting tumor growth. Consistent with the previously reported results [19], tumors grew to approximately 1 cm within 1 week post-implantation, enabling simultaneous C-13 MRS/PET/mpMR imaging and multimodal image fusion-guided targeted biopsy procedures within 2 weeks of tumor implantation, thereby avoiding animal distress for a prolonged duration. Interestingly, and in contrast to the previous report which only showed signs of chronic lymphoplasmacytic prostatitis on histology [19], acute prostatitis with focal areas of even severe inflammatory cell infiltrations was a dominant histological feature in our study; in dog 1, only scattered nests and clusters of tumor cells were observed on histology with severe inflammatory cell infiltrations in the area of tumor cell implantation, likely reflecting acute rejection despite therapeutic doses of cyclosporine. BPH was not observed in any of the animals, likely due to the relatively young age of the dogs. We acknowledge that this model did not reflect the tumor microenvironment of human PCa and the magnitude of measured imaging signals in tumor and control tissue was possibly confounded by the presence of moderate to severe concomitant inflammation and necrosis and, thus, may be different in human patients.

PET signal attenuation by the clamshell coil was measured and attenuation-corrected PET reconstructions were employed for subsequent *in vivo* imaging experiments. We first used [^{18}F]FDG expecting substantial metabolic activity in fast-growing orthotopic PCa model, which was confirmed in our study. However, since [^{18}F]FDG has a limited role in clinical PCa imaging due to its low glucose metabolism and non-specific uptake in benign conditions, we also tested the bombesin-like GRPR-binding peptide ^{68}Ga-NODAGA-SCH1 in one of the dogs. GRPR is emerging as a novel imaging target because it is highly expressed in PCa with substantially lower expression levels in benign conditions like BPH and inflammation [25]. [^{68}Ga]NODAGA-SCH1 has shown high stability and tumor uptake in human prostate adenocarcinoma PC3 xenografts in mice [26]. In this study, we demonstrated high GRPR expression on canine Ace-1 cells and differential [^{68}Ga]NODAGA-SCH1 uptake *in vivo* in canine PCa compared to normal prostate tissue in one dog. A next-generation synthetic bombesin receptor antagonist, ^{68}Ga-labeled DOTA-4-amino-1-carboxymethyl-piperidine-D-Phe-Gln-Trp-Ala-Val-Gly-His-Sta-Leu-NH2 ([^{68}Ga]RM2 or [^{68}Ga]DOTA-Bombesin, formerly also known as BAY86-7548), has recently been clinically translated [18, 27] and shown promising results compared to PSMA-targeted PET imaging in patients with recurrent PCa [18].

While proton (^{1}H) MRS imaging has been explored extensively for detecting PCa based on measurement of choline-to-citrate ratio, these metabolites are present in very small concentrations requiring long data acquisition times and resulting in limited spatial resolution [28]. Through hyperpolarization, signal-to-noise ratio could be substantially improved in hyperpolarized C-13 MRS imaging compared to (^{1}H) MRS imaging [13]. Recently, hyperpolarized [1-^{13}C]Pyr has been used in a first-in-human clinical trial [16]. This phase I trial of 31 patients with biopsy-proven localized PCa had several important findings. The bolus injection of hyperpolarized [1-^{13}C]Pyr was shown to be safe, with no dose-limiting toxicities. Elevated [1-^{13}C]Lac/[1-^{13}C]Pyr ratios were observed within biopsy-proven cancer lesions. Specifically, hyperpolarized C-13 MRS imaging was able to distinguish tumor from normal prostate, with Pyr to Lac conversion ~4–5 times higher in tumors, consistent with preclinical studies [17, 29]. One case identified a region, missed by mpMRI, with an elevated [1-^{13}C]Lac/[1-^{13}C]Pyr ratio (proven as cancer by subsequent biopsy). With a clinical hyperpolarizer located adjacent to our PET/MR scanner, simultaneous hyperpolarized C-13 MRS along with PET and mpMR imaging was shown to be feasible.

Fusing mpMRI with TRUS has emerged as a powerful tool to enable image-targeted prostate biopsy [8, 9]. It significantly reduces missed high-grade cancer [30] and is a recommended method for patient selection for focal therapy [31]. Also, fusion improved the detection of PCa, particularly in men with prior negative conventional prostate biopsies [4, 32]. However, mpMRI has its own limitations [11, 33]. A recent meta-analysis of seven studies with 526 patients who underwent prostatic mpMRI showed a specificity of 88 % and sensitivity of 74 % with negative predictive value ranging from 65 to 94 % for PCa detection [34]. In a retrospective study of patients with prostate lesions suspected as likely ($n = 373$, PI-RADS 4) or highly likely ($n = 528$, PI-RADS 5) to be aggressive PCa, in-bore MRI-guided prostate biopsy detected no cancer in 40.2 and 9.3 % of patients, respectively [35]. Our study showed that fusion of multimodality imaging data set is feasible along with a successful image fusion-guided biopsy. Future studies in patients are warranted to assess whether multimodal imaging improves biopsy yields, minimizes the number of biopsies to diagnose and characterize PCa, and whether this approach is cost-efficient.

Our study had the following limitations. While canine tumor model allowed assessing feasibility of multimodality imaging, as discussed above, the tumor model does not simulate the biology of human PCa. Therefore, SUV and Lac/totalC ratio values in this study are considered descriptive and will need to be restudied when scaling to patients. Moreover, we observed increased Lac labeling in areas with inflammation in contralateral prostate of dogs 2 and 3 in levels similar to the tumor, leading to a non-specific false-positive signal. A similar increased Pyr to Lac exchange had also been noted in other studies to specifically identify inflammation [36–38], suggesting that the PCa diagnosis based solely on [1-^{13}C]Pyr to [1-^{13}C]Lac label flux in the face of prostatitis needs to be investigated further. Furthermore, hyperpolarized C-13 MRS imaging was performed in 2D only with a single plane acquired over the suspected area of tumors. Therefore, this portion of the multimodal data sets could not be fused with TRUS for guided biopsy at the time of this study. A 3D echo-planar hyperpolarized C-13 spectroscopic imaging pulse sequence has been developed [16] that allows volumetric evaluation of the entire prostate and, thus, also fusion with TRUS in the future. Lastly, as the tumors were of canine origin and biologically different from human PCa, differences in imaging signal based on tumor aggressiveness cannot be evaluated in this study. Future clinical studies are warranted to assess whether multimodality imaging improves differentiation of indolent from aggressive PCa.

Conclusions

In conclusion, the results of our study suggest that simultaneous hyperpolarized C-13 MRS/PET/mpMR imaging is feasible in a canine model of PCa. Tumors were visualized at least by one imaging modality, indicating the potential benefit of a multimodality approach for PCa imaging. This study lays the foundation for a future clinical assessment of this approach evaluating the combined performance of various promising imaging techniques to detect and characterize PCa in patients.

Acknowledgments. The canine PCa cells (Ace-1) were obtained from Dr. Thomas Rosol, Department of Veterinary Biosciences, Ohio State University. We would like to thank Philips for providing the EPIQ7 ultrasound system, C10-4ec transducer, and PercuNav image fusion software. We thank Praveen Gulaka, Valentina Taviani, Dawn Holley, and Harsh Gandhi for their assistance with PET/MR acquisition and reconstruction; Jim Strommer for help with Fig. 1; Don Samaan from Health Physics; veterinary service center staff; and members of Willmann, Spielman, Cheng labs, and Frezghi Habte who helped with this study.

Compliance with Ethical Standards. The Institutional Animal Care and Use Committee approved all procedures in this study.

Conflict of Interest

The authors declare that they have no conflict of interest.

References

1. Siegel RL, Miller KD, Jemal A (2016) Cancer statistics, 2016. CA Cancer J Clin 66:7–30
2. Wagenlehner FME, Van Oostrum E, Tenke P et al (2013) Infective complications after prostate biopsy: outcome of the Global Prevalence Study of Infections in Urology (GPIU) 2010 and 2011, a prospective multinational multicentre prostate biopsy study. Eur Urol 63:521–527
3. Loeb S, Bjurlin MA, Nicholson J, Tammela TL, Penson DF, Carter HB, Carroll P, Etzioni R (2014) Overdiagnosis and overtreatment of prostate cancer. Eur Urol 65:1046–1055
4. Sonn GA, Chang E, Natarajan S, Margolis DJ, Macairan M, Lieu P, Huang J, Dorey FJ, Reiter RE, Marks LS (2014) Value of targeted prostate biopsy using magnetic resonance-ultrasound fusion in men with prior negative biopsy and elevated prostate-specific antigen. Eur Urol 65:809–815
5. Johnson LM, Turkbey B, Figg WD, Choyke PL (2014) Multiparametric MRI in prostate cancer management. Nat Rev Clin Oncol 11:346–353
6. Cash H, Maxeiner A, Stephan C, Fischer T, Durmus T, Holzmann J, Asbach P, Haas M, Hinz S, Neymeyer J, Miller K, Günzel K, Kempkensteffen C (2016) The detection of significant prostate cancer is correlated with the Prostate Imaging Reporting and Data System (PI-RADS) in MRI/transrectal ultrasound fusion biopsy. World J Urol 34:525–532
7. Park SY, Jung DC, Oh YT et al (2016) Prostate cancer: PI-RADS version 2 helps preoperatively predict clinically significant cancers. Radiology 280:151133–151133
8. Pinto PA, Chung PH, Rastinehad AR, Baccala AA Jr, Kruecker J, Benjamin CJ, Xu S, Yan P, Kadoury S, Chua C, Locklin JK, Turkbey B, Shih JH, Gates SP, Buckner C, Bratslavsky G, Linehan WM, Glossop ND, Choyke PL, Wood BJ (2011) Magnetic resonance imaging/ultrasound fusion guided prostate biopsy improves cancer detection following transrectal ultrasound biopsy and correlates with multiparametric magnetic resonance imaging. J Urol 186:1281–1285
9. Filson CP, Natarajan S, Margolis DJA, Huang J, Lieu P, Dorey FJ, Reiter RE, Marks LS (2016) Prostate cancer detection with magnetic resonance-ultrasound fusion biopsy: the role of systematic and targeted biopsies. Cancer 122:884–892

10. Le JD, Tan N, Shkolyar E et al (2015) Multifocality and prostate cancer detection by multiparametric magnetic resonance imaging: correlation with whole-mount histopathology. Eur Urol 67:569–576
11. Priester A, Natarajan S, Khoshnoodi P et al (2016) Magnetic resonance imaging underestimation of prostate cancer geometry: use of patient-specific molds to correlate images with whole-mount pathology. J Urol 197:320–326
12. Wilson DM, Kurhanewicz J (2014) Hyperpolarized ^{13}C MR for molecular imaging of prostate cancer. J Nucl Med 55:1567–1572
13. Hurd RE, Yen YF, Chen A, Ardenkjaer-Larsen JH (2012) Hyperpolarized ^{13}C metabolic imaging using dissolution dynamic nuclear polarization. J Magn Reson Imaging 36:1314–1328
14. Day SE, Kettunen MI, Fa G et al (2007) Detecting tumor response to treatment using hyperpolarized ^{13}C magnetic resonance imaging and spectroscopy. Nat Med 13:1382–1387
15. Gutte H, Hansen AE, Johannesen HH, Clemmensen AE, Ardenkjær-Larsen JH, Nielsen CH, Kjær A (2015) The use of dynamic nuclear polarization ^{13}C-pyruvate MRS in cancer. Am J Nucl Med Mol Imaging 5:548–560
16. Nelson SJ, Kurhanewicz J, Vigneron DB et al (2013) Metabolic imaging of patients with prostate cancer using hyperpolarized [1-^{13}C]pyruvate. Sci Transl Med 5:198ra108–198ra108
17. Albers MJ, Bok R, Chen AP, Cunningham CH, Zierhut ML, Zhang VY, Kohler SJ, Tropp J, Hurd RE, Yen YF, Nelson SJ, Vigneron DB, Kurhanewicz J (2008) Hyperpolarized ^{13}C lactate, pyruvate, and alanine: noninvasive biomarkers for prostate cancer detection and grading. Cancer Res 68:8607–8615
18. Minamimoto R, Hancock S, Schneider B, Chin FT, Jamali M, Loening A, Vasanawala S, Gambhir SS, Iagaru A (2016) Pilot comparison of ^{68}Ga-RM2 PET and ^{68}Ga-PSMA-11 PET in patients with biochemically recurrent prostate cancer. J Nucl Med 57:557–562
19. Keller JM, Schade GR, Ives K, Cheng X, Rosol TJ, Piert M, Siddiqui J, Roberts WW, Keller ET (2013) A novel canine model for prostate cancer. Prostate 73:952–959
20. Gutte H, Hansen AE, Larsen MM et al (2015) Simultaneous hyperpolarized ^{13}C-pyruvate MRI and ^{18}F-FDG PET (HyperPET) in 10 dogs with cancer. J Nucl Med 56:1786–1792
21. Leroy BE, Northrup N (2009) Prostate cancer in dogs: comparative and clinical aspects. Vet J 180:149–162
22. Coffey DS, Walsh PC (1990) Clinical and experimental studies of benign prostatic hyperplasia. Urol Clin North Am 17:461–475
23. Waters DJ, Bostwick DG (1997) The canine prostate is a spontaneous model of intraepithelial neoplasia and prostate cancer progression. Anticancer Res 17:1467–1470
24. Smith J (2008) Canine prostatic disease: a review of anatomy, pathology, diagnosis, and treatment. Theriogenology 70:375–383
25. Markwalder R, Reubi JC (1999) Gastrin-releasing peptide receptors in the human prostate: relation to neoplastic transformation. Cancer Res 59:1152–1159
26. Sun Y, Ma X, Zhang Z, Sun Z, Loft M, Ding B, Liu C, Xu L, Yang M, Jiang Y, Liu J, Xiao Y, Cheng Z, Hong X (2016) Preclinical study on GRPR-targeted 68Ga-probes for PET imaging of prostate cancer. Bioconjug Chem 27:1857–1864
27. Roivainen A, Kahkonen E, Luoto P, Borkowski S, Hofmann B, Jambor I, Lehtio K, Rantala T, Rottmann A, Sipila H, Sparks R, Suilamo S, Tolvanen T, Valencia R, Minn H (2013) Plasma pharmacokinetics, whole-body distribution, metabolism, and radiation dosimetry of ^{68}Ga bombesin antagonist BAY 86-7548 in healthy men. J Nucl Med 54:867–872
28. Podo F, Serkova NJ, Nelson S, Brindle KM, Serrao EM (2016) Potential clinical roles for metabolic imaging with hyperpolarized [1-^{13}C]pyruvate. Front Oncol 6:593389–593359
29. Keshari KR, Sriram R, Van Criekinge M et al (2013) Metabolic reprogramming and validation of hyperpolarized ^{13}C lactate as a prostate cancer biomarker using a human prostate tissue slice culture bioreactor. Prostate 73:1171–1181
30. Siddiqui MM, Rais-Bahrami S, Turkbey B, George AK, Rothwax J, Shakir N, Okoro C, Raskolnikov D, Parnes HL, Linehan WM, Merino MJ, Simon RM, Choyke PL, Wood BJ, Pinto PA (2015) Comparison of MR/ultrasound fusion-guided biopsy with ultrasound-guided biopsy for the diagnosis of prostate cancer. J Am Med Assoc 313:390–397
31. Donaldson Ia AR, Barratt D et al (2014) Focal therapy: patients, interventions, and outcomes—a report from a consensus meeting. Eur Urol 67:771–777
32. Sonn GA, Natarajan S, Margolis DJA, MacAiran M, Lieu P, Huang J, Dorey FJ, Marks LS (2013) Targeted biopsy in the detection of prostate cancer using an office based magnetic resonance ultrasound fusion device. J Urol 189:86–91
33. Sosnowski R, Zagrodzka M, Borkowski T (2016) The limitations of multiparametric magnetic resonance imaging also must be borne in mind. Cent Eur J Urol 69:22–23
34. De Rooij M, Hamoen EHJ, Fütterer JJ et al (2014) Accuracy of multiparametric MRI for prostate cancer detection: a meta-analysis. Am J Roentgenol 202:343–351
35. Venderink W, van Luijtelaar A, Bomers JG et al (2017) Results of targeted biopsy in men with magnetic resonance imaging lesions classified equivocal, likely or highly likely to be clinically significant prostate cancer. Eur Urol 73:353–360
36. MacKenzie JD, Yen Y-F, Mayer D, Tropp JS, Hurd RE, Spielman DM (2011) Detection of inflammatory arthritis by using hyperpolarized ^{13}C-pyruvate with MR imaging and spectroscopy. Radiology 259:414–420
37. Najac C, Chaumeil MM, Kohanbash G, Guglielmetti C, Gordon JW, Okada H, Ronen SM (2016) Detection of inflammatory cell function using 13C magnetic resonance spectroscopy of hyperpolarized [6-^{13}C]-arginine. Sci Rep 6:31397
38. Shaghaghi H, Kadlecek S, Deshpande C, Siddiqui S, Martinez D, Pourfathi M, Hamedani H, Ishii M, Profka H, Rizi R (2014) Metabolic spectroscopy of inflammation in a bleomycin-induced lung injury model using hyperpolarized 1-^{13}C pyruvate. NMR Biomed 27:939–947